Journal of ELECTRONIC MATERIALS, Vol. 46, No. 6, 2017
DOI: 10.1007/s11664-017-5489-6

Thermal Evaporation Synthesis and Optical Properties of ZnS Microbelts on Si and Si/SiO_2 Substrates

V.N. NGUYEN,[1] N.T. KHOI,[1] and D.H. NGUYEN [1,2]

1.—Advanced Institute for Science and Technology (AIST), Hanoi University of Science and Technology (HUST), 01 Dai Co Viet, Hanoi, Vietnam. 2.—e-mail: hung.nguyenduy@hust.edu.vn

In this study, we report on the differences in optical properties of zinc sulfide (ZnS) microbelts grown on Si and Si/SiO_2 substrates by a thermal evaporation method. Our investigation suggests that the composition and luminescence of the microbelts are dependent on the growth substrate. Field emission scanning electron microscopy images show the formation of nanoparticles with a diameter of 300–400 nm on ZnS microbelts grown on Si substrate. In addition, energy dispersive x-ray spectroscopy analysis combined with x-ray diffraction and Raman measurements reveal the existence of Si on these microbelts which may bond with O to form SiO_2 or amorphous silica. In contrast, no Si presents on the microbelts grown on Si/SiO_2 substrate. Moreover, photoluminescence measurement at 300 K shows a narrow emission peak in the near-ultraviolet region from microbelts grown on Si/SiO_2 substrate but a broad emission band with multi-peaks from microbelts grown on Si substrate. The origin of the luminescence distinction between microbelts is discussed in terms of the differences in the growth substrates and compositions.

Key words: ZnS microbelts, thermal evaporation, Si substrate, photoluminescence

INTRODUCTION

Wide-band-gap semiconductors have attracted considerable attention because of their possible applications in optoelectronic devices, energy conversion devices, and transparent conducting electrodes, thanks to their excellent electronic, optical, and thermal properties.[1,2] While III–V compound semiconductors have already found many applications in optoelectronics devices such as light-emitting diodes, solar cells, and displays, II–VI compounds are still under development and have been actively studied in recent years.[3,4] ZnS is a direct wide-band-gap II–VI semiconductor with a high refractive index and significant transmittance in the visible range of the electromagnetic spectrum with band gaps of 3.72 eV and 3.77 eV for cubic zincblende and hexagonal wurtzite crystal structures, respectively. ZnS has recently garnered much interest because of the nanostructures which have a large surface–volume ratio.[5] Various nanostructures of ZnS, including nanowires, nanoribbons, nanocombs, nanorods, and nanobelts, have been synthesized by different methods such as chemical vapor deposition,[6] molecular-beam epitaxy,[7] metal–organic chemical vapor deposition,[8] hydrothermal methods,[9] pulsed laser deposition,[10] and thermal evaporation.[11–14] Among those available techniques, the thermal evaporation and vapor-phase transport methods have been extensively used because well-formed nanostructures with high crystalline quality can be grown in a simple, cost-effective, and scalable way.[14–16] The thermal evaporation method seems to be favored for high-temperature growth in most cases.[11–14] For practical applications, ZnS nanostructures have been usually grown on Si and Si/SiO_2 substrates because they are relatively inexpensive and appropriate for use in Si-based photonic devices.[8,11,12,15,16] In fact, ZnS nanostructures grown on these different substrates have significantly different morphologies.[17] However, ZnS is easily oxidized into ZnO as a nanostructure. To

(Received October 1, 2016; accepted March 28, 2017; published online April 6, 2017)

date, several groups have achieved ZnS encapsulated inside hollow cavities of silica nanotubes, which can be used as sheaths to prevent oxidation of semiconductor nanowires or to avoid interference in the building blocks of a complex nanoscale circuit.[18–20] Furthermore, SiO_2 can modulate the physical and chemical properties of ZnS, hence improving the performance of the devices. However, information on the effects of the Si/SiO_2 and Si substrates on the optical properties of ZnS is still limited and the underlying mechanism is not well understood.

In this work, we report the synthesis of ZnS microbelts on Si substrates with and without a SiO_2 top layer. The effects of the substrate on the morphology, composition, and optical properties of the microbelts have been investigated. Interestingly, the byproduct silica forms on the microbelts grown on the Si substrate and amorphous SiO_2 modified the luminescence of ZnS microbelts compared with that on the Si/SiO_2 substrate. Specifically, the former shows a broad emission band with multi-peaks in contrast with a sharp peak from the latter. This result may inspire great interest in exploring SiO_2-based nanostructures and their potential applications in future integrated devices.

EXPERIMENTAL

Synthesis of ZnS Microbelts

ZnS microbelts were synthesized by thermal evaporation of ZnS nanopowders in a conventional horizontal tube furnace. A Si wafer was oxidized at 1050°C for 4 h to create a SiO_2 layer on the substrate. For another Si wafer, the native SiO_2 layer was removed by HF solution for 30 min. Then, a 10-nm Au layer was sputtered on the substrates to serve as seeds for growing nanorods. An amount of 0.5 g ZnS nanopowder (purity: 99.999%) with average size of 2–4 nm was located in an alumina boat and then inserted into a quartz tube inside the furnace. The position of the boat was kept at the center of the tube to guarantee uniform temperature distribution along it. The Au-coated Si/SiO_2 and Si trips with a size of 1 cm × 2 cm were placed downstream in the quartz tube for material growth onto subsequent thermal evaporation steps. The quartz tube was initially purged with pure argon for 60 min, and then heated at a rate of 10°C per min under a constant flow of 100 sccm Ar gas and held at 200°C for 10 min. After that, the temperature was raised to 1170°C and kept there for 30 min while the Ar gas flow rate was reduced to 50 sccm. Finally, the furnace was naturally cooled to room temperature.

Characterization

The morphology, microstructure, chemical composition, and optical properties of the ZnS nanostructures were examined using field emission scanning electron microscopy (FESEM) (Jeol JSM-7600F) combined with energy dispersive x-ray spectroscopy (EDS) (Oxford Instruments X-Max 50). The structure and crystallinity were examined and analyzed by x-ray diffraction (XRD) (Siemens D5000). The synthesized material was characterized by Raman spectroscopy (LabRAM HR Evolution). The continuous wave photoluminescence (PL) spectra were recorded on Horiba Jobin–Yvon Nano-Log spectrometers using a Xenon lamp (450 W) as an excitation source.

RESULTS AND DISCUSSION

The general morphology of the ZnS microbelts on the Si and Si/SiO_2 substrates is shown in Fig. 1a–d, which demonstrates that they grow horizontally and take random directions on the substrate. The microbelts with average diameter of 5–7 μm and length of several tens of μm were grown on the Si and Si/SiO_2 wafers with quite high density. Note that the surface of microbelts grown on the Si/SiO_2 substrate is smooth but there are nanoparticles with diameter of 300–500 nm on the surface of the ZnS microbelts grown on the Si substrate.

The composition of a single ZnS microbelt deposited on Si and Si/SiO_2 substrates was examined by EDS and is shown in Fig. 1e and f. The ZnS microbelt grown on the Si/SiO_2 substrate has the chemical composition of 48.0 at.% Zn, 45.5 at.% S, and 6.5 at.% O. Nonetheless, the measurement on the ZnS microbelts grown on Si substrate confirms the chemical composition of 10.6 at.% Zn, 9.8 at.% S, 53.9 at.% O, and 26.1 at.% Si. Si composition on ZnS microbelts originates from the substrate surface and its formation is via direct absorption of the silica gas phase or silica moved up along the ZnS microbelts from their base.[21,22]

To determine the crystalline phase of ZnS and silica, XRD measurement was performed. Figure 2 shows the XRD patterns, identifying the phases of ZnS crystals. The ZnS microbelts grown in the Si and Si/SiO_2 substrates are matched to the structure of wurtzite (JCPDS 05-0492). However, the XRD pattern of the product grown on the Si substrate shows a low intensity and broad peak at $2\theta = 21.5°$. It can be seen from the XRD pattern that the broadening is assigned to the SiO_2 peak caused by small crystalline size effect or amorphous silica.[23] In this case, the Si composition comes from the substrate, while oxygen is likely originated from oxygen in air which diffused into the tube from the opened end of the tube furnace. Nonetheless, no peak shift is observed when comparing the peak position of the crystalline phase of ZnS grown on Si with the one on the Si/SiO_2 substrate. This result reveals that Si may be not inserted into the ZnS crystal lattice.

Furthermore, Raman spectra (100–950 cm^{-1}) of the ZnS microbelts were collected in air and at room temperature. Most peaks can be readily assigned to hexagonal ZnS crystalline.[24,25] As shown in Fig. 3, there is no peak shift between the samples. At low

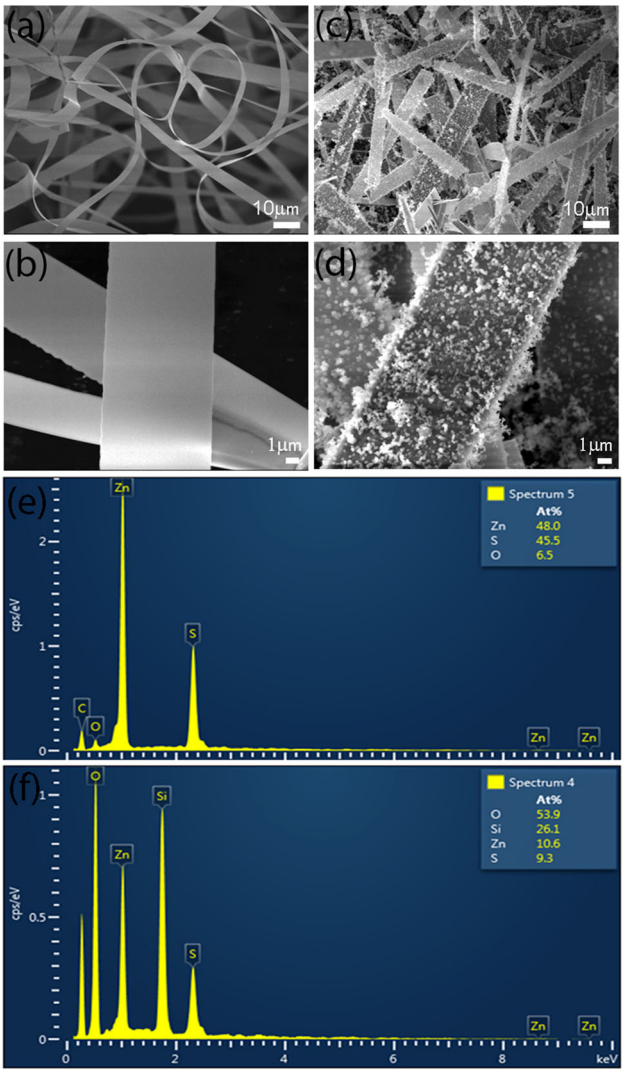

Fig. 1. Top view of FESEM images with low and high magnification of microbelts grown on Si/SiO_2 substrate (a, b) and Si substrate (c, d). EDS spectra of ZnS microbelts, separated from the substrates, grown on Si/SiO_2 substrate (e) and Si substrate (f).

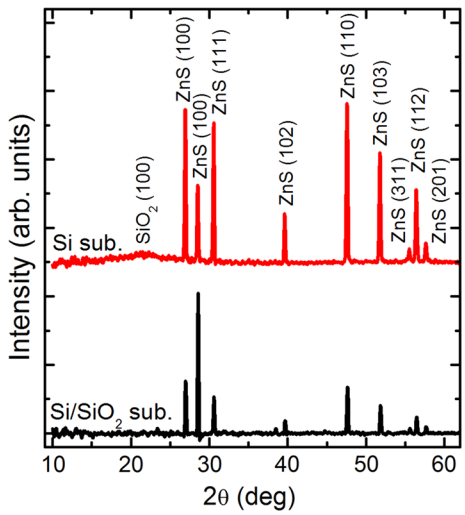

Fig. 2. XRD pattern of ZnS microbelts grown on Si/SiO_2 and Si substrates.

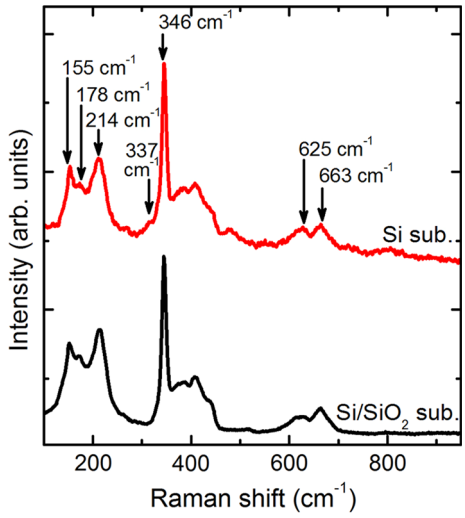

Fig. 3. Raman spectra of ZnS microbelts grown on Si/SiO_2 and Si substrates.

frequency, the peaks at 155 cm^{-1} and 178 cm^{-1} are assigned as disorder-activated second-order acoustic phonons.[22,23] The possibility of observing these features from ZnS microbelts may be due to the surface enhancement effect promoted by the metal particles.[26] The peak centered at 214 cm^{-1} is assigned to a first-order LA mode. The peak at 337 cm^{-1}, which is not seen from the ZnS crystal, is due to optical phonon scattering related to bonding between S and O (SO).[5,27,28] A strong scattering at 346 cm^{-1} is identified with A_1/E_1 of LO modes.[26–29] The continuum scattering in the range 350–450 cm^{-1} is due to the combination of the TO + TA, LO + TA, LO + LA phonon modes.[28] The strong broad Raman bands between 625 cm^{-1} and 663 cm^{-1} can be assigned to the TO + LA and 2LO modes.[28] The intensity ratio of the second-order LO to first-order LO phonon responses is closely related to the crystalline quality and/or exciton–LO phonon coupling strength.[29] The intensity ratios of the second-order LO to first-order LO phonons among the ZnS microbelts are nearly the same, suggesting that there is no significant change in the crystalline quality and/or exciton–LO phonon coupling strength among the ZnS microbelts.

The PL spectra of ZnS microbelts grown on Si and Si/SiO_2 substrates were measured at 10 K using a 270-nm excitation wavelength as shown in Fig. 4a. There are four prominent emission peaks appearing in all samples at 334 nm, 366 nm, 465 nm, and 574 nm. The lowest peak at 334 nm is ascribed to the band-to-band transition of ZnS. The peak at 366 nm seems to result from the near band edge emission of ZnO. The peaks at 460 nm and 574 nm are attributed to luminescence centers of ZnS and ZnO.[30] In Fig. 4b, the PL spectrum of ZnS microbelts grown on Si/SiO_2 substrate carried out at 300 K shows a peak at 377 nm and a broad emission band peaking at 500 nm. The peak at 377 nm is due

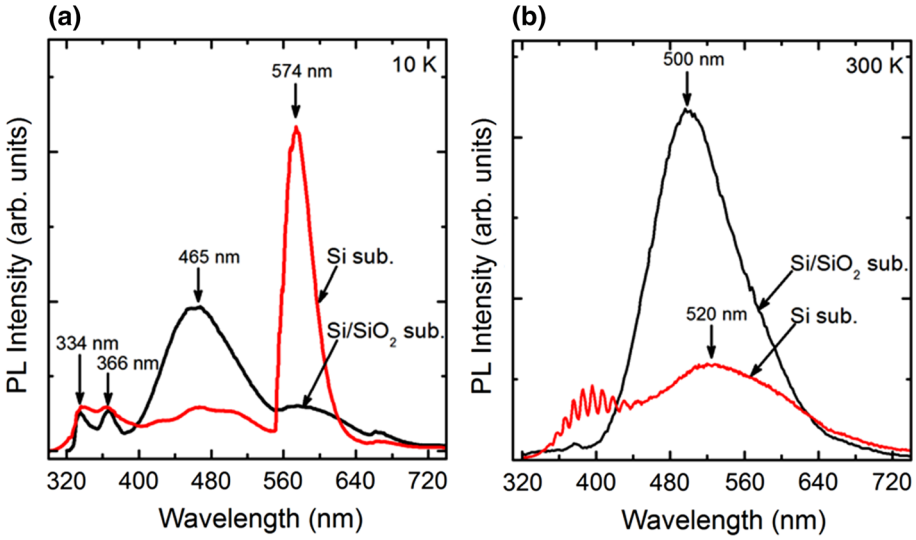

Fig. 4. PL spectra of ZnS microbelts grown on Si/SiO_2 and Si substrates at 10 K (a) and 300 K (b) under excitation wavelength of 270 nm.

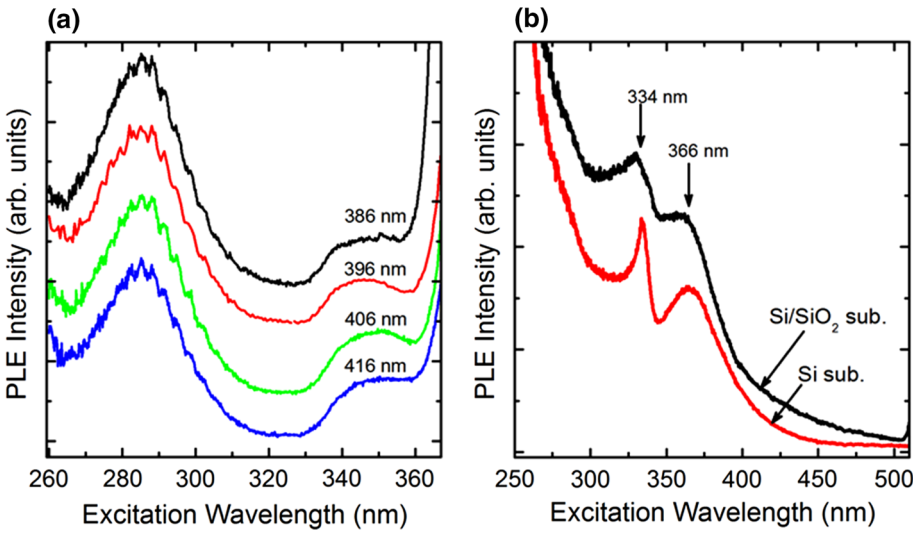

Fig. 5. PLE spectra of ZnS microbelts grown on Si substrate at 300 K monitored at emission peaks 386 nm, 396 nm, 406 nm, and 416 nm (a). PLE spectra of ZnS microbelts grown on Si/SiO_2 and Si substrates at 300 K monitored at emission peaks 500 nm and 520 nm, respectively (b).

to the near band edge emission of ZnO nanocrystals.[31] In contrast, the PL spectrum of ZnS microbelts grown on the Si substrate present multi-peaks at 348 nm, 358 nm, 366 nm, 376 nm, 386 nm, 396 nm, 406 nm, 416 nm, 430 nm, and 443 nm and a broad emission band peaking at 520 nm. The multi-peaks have yet to be reported in ZnS and ZnO nanostructures. In addition, some studies on alloyed or composited Si-ZnS reported only a broad emission band near the ultra-violet (UV) region.[19,20] To determine the origin of the peaks, PL excitation (PLE) measurements were carried out at several peaks. Figure 5a shows the PLE spectra monitored at the selected emission peaks of 386 nm, 396 nm, 406 nm, and 416 nm. The spectra show a peak at 285 nm and a broad band from 340 nm to 360 nm. The broad excitation peak at 285 nm could be attributed to the surface defects such as oxygen vacancies or non-bridge oxygen hole centers induced by silica.[32–34] The other broad band from 340 nm to 360 nm was attributed to the relaxation of carriers from the near band edge and the shallow centers of ZnS. From the analysis of the PL and PLE spectra of the microbelts grown on the Si substrate, the multi-peak emission near the UV region may be due to interference effects, which were created by SiO_2 or silica implanted with Zn^+ or S^+.[35,36] In the visible region, the emission peak at 574 nm, which appears at 10 K, disappears at 300 K which may be due to the recapture of the carrier from lower to higher energy centers or by nonradiative traps. Meanwhile, the green emission peaks at 500 nm and 520 nm (Fig. 4b) are observed at 300 K for microbelts grown on the Si/SiO_2 and Si substrates,

respectively. These emission peaks may be assigned to the surface defects such as oxygen vacancies induced by the silica.[18] In fact, PLE spectra for these emission peaks show two bands centered at 334 nm and 366 nm, as shown in Fig. 5b. This indicates that the carriers transfer from the near band edge of ZnS and ZnO to the luminescence centers formed by S^{2-}, O^{2-}, and Zn^{2+} in ZnS and ZnO.[29,37] These centers are due to the appearance of O and the difference of the atomic ratio between Zn and S which is confirmed by EDS analysis.

CONCLUSION

ZnS microbelts on Si and Si/SiO_2 substrates have been successfully synthesized by a thermal evaporation method. The morphology of the microbelts is not influenced significantly by the SiO_2 layer on the Si substrate. However, silica exists, which forms on the microbelts grown on the Si substrate via direct absorption of the silica gas phase or silica moved up the ZnS microbelts from their base. The existence of the amorphous SiO_2 on the microbelts affects their luminescence. Specifically, the PL spectrum at room temperature of the ZnS microbelts with amorphous SiO_2 shows a multi-peak emission in the near-UV region. Based on the analysis of the PL and PLE spectra, it can be concluded that the luminescence band can be attributed to the surface defects such as oxygen vacancies induced by the silica. The UV emissions of the as-grown product are of significant interest for their potential applications in future integrated devices.

ACKNOWLEDGEMENT

This research is funded by the Hanoi University of Science and Technology under Grant Number T2016-PC-016.

REFERENCES

1. S. Kasap and P. Capper, *Springer Handbook of Electronic and Photonic Materials* (New York: Springer, 2006).
2. K. Takahashi, A. Yoshikawa, and A. Sandhu, *Wide Bandgap Semiconductors: Fundamental Properties and Modern Photonic and Electronic Devices* (Berlin: Springer, 2007).
3. R. Bhargava, *Properties of Wide Bandgap II-V Semiconductors* (INSPEC, The Insititution of Electrical Engineers, 1997).
4. X. Fang, Y. Bando, U.K. Gautam, T. Zhai, H. Zeng, X. Xu, M. Liao, and D. Golberg, *Crit. Rev. Solid State Mater. Sci.* 34, 190 (2009).
5. X. Fang, T. Zhai, U.K. Gautam, L. Li, L. Wu, Y. Bando, and D. Golberg, *Prog. Mater Sci.* 56, 175 (2011).
6. M. Lei, X.L. Fu, P.G. Li, and W.H. Tang, *J. Alloys Compd.* 509, 5769 (2011).
7. S.K. Lok, G. Wang, Y. Cai, N. Wang, Y.C. Zhong, K.S. Wong, and I.K. Sou, *J. Cryst. Growth* 311, 2630 (2009).
8. S.C. Kim, J.W. Kim, H.S. Chung, D.H. Kim, and K.H. Oh, *J. Korean Phys. Soc.* 55, 978 (2009).
9. D.D.D. Ma and S.T. Lee, *Nano Lett.* 6, 296 (2006).
10. Q. Xiong, G. Chen, J.D. Acord, X. Liu, J.J. Zengel, H.R. Gutierrez, J.M. Redwing, L.C.L.Y. Voon, B. Lassen, and P.C. Eklund, *Nano Lett.* 4, 1663 (2004).
11. Q. Li and C. Wang, *Appl. Phys. Lett.* 83, 359 (2003).
12. B.Y. Geng, X.W. Liu, Q.B. Du, X.W. Wei, and L.D. Zhang, *Appl. Phys. Lett.* 88, 163104 (2006).
13. G.Z. Shen, Y. Bando, J.Q. Hu, and D. Golberg, *Appl. Phys. Lett.* 90, 123101 (2007).
14. J.X. Ding, J.A. Zapien, W.W. Chen, Y. Lifshitz, S.T. Lee, and X.M. Meng, *Appl. Phys. Lett.* 85, 2361 (2004).
15. H.Y. Yang, S.F. Yu, J. Yan, and L.D. Zhang, *Nanoscale Res. Lett.* 5, 809 (2010).
16. H. Zhu, S.C. Su, and S.F. Yu, *IEEE J Top. Quantum Electron.* 19, 150175 (2013).
17. Y. Li, C.H. Ye, X. Fang, L. Yang, Y. Xiao, and L. Zhang, *Nanotechnology* 16, 501 (2005).
18. H. Tang, B.J. Kwon, J. Kim, and J.Y. Park, *J. Phys. Chem. C* 114, 21366 (2010).
19. M. Nilkar, F.E. Ghodsi, and A. Abdolahzadeh Ziabari, *Appl. Phys. A* 118, 1377 (2015).
20. Y. Chen, Q. Zhou, X. Zhang, Y. Su, C. Jia, Q. Li, and W. Kong, *Cryst. Growth Des.* 9, 728 (2009).
21. Q. Li and C. Wang, *J. Am. Chem. Soc.* 125, 9892 (2003).
22. H.W. Kim, H.S. Kim, H.G. Na, J.C. Yang, J.K. Jeong, C. Lee, and D.Y. Kim, *J. Solid State Chem.* 183, 2490 (2010).
23. D. Moore, J.R. Morber, R.L. Snyder, and Z.L. Wang, *J. Phys. Chem. C* 112, 2895 (2008).
24. S.M. Scholz, R. Vacassy, L. Lemaire, J. Dutta, and H. Hofmann, *Appl. Organomet. Chem.* 12, 327 (1998).
25. M. Abdulkhadar and B. Thomas, *Nanostruct. Mater.* 5, 289 (1995).
26. M. Lin, T. Sudhiranjan, C. Boothroyd, and K.P. Loh, *Chem. Phys. Lett.* 400, 175 (2004).
27. Q. Xiong, J. Wang, O. Reese, L.C.L.Y. Voon, and P.C. Eklund, *Nano Lett.* 4, 1991 (2004).
28. J.H. Kim, H. Rho, J. Kim, Y.-J. Choi, and J.-G. Park, *J. Raman Spectrosc.* 43, 906 (2012).
29. Z.G. Chen, L. Cheng, and J. Zou, *CrystEngComm* 13, 5885 (2011).
30. J. Yan, X. Fang, L. Zhang, Y. Bando, U.K. Gautam, B. Dierre, T. Sekiguchi, and D. Golberg, *Nano Lett.* 8, 2794 (2008).
31. D.Q. Trung, N. Tu, N.D. Hung, and P.T. Huy, *J. Lumin.* 169, 165 (2016).
32. M. Leone, S. Agnello, R. Boscaino, M. Cannas, and F.M. Gelardi, *Phys. Rev. B* 60, 11475 (1999).
33. X.J. Hao, A.P. Podhorodecki, Y.S. Shen, G. Zatryb, J. Misiewicz, and M.A. Green, *Nanotechnology* 20, 485703 (2009).
34. Z.T. Kang, B. Arnold, C.J. Summers, and B.K. Wagner, *Nanotechnology* 17, 4477 (2006).
35. E.A. Buntov, A.F. Zatsepin, A.I. Slesarev, A.P. Mikhailovich, and A.N. Mikhaylov, *Phys. Status Solidi A* 212, 2672 (2015).
36. E.A. Buntov, A.F. Zatsepin, V.S. Kortov, V.A. Pustovarov, and H.-J. Fitting, *J. Non Cryst. Solids* 357, 1977 (2011).
37. M. Hafeez, S. Rehman, U. Manzoor, M.A. Khan, and A.S. Bhatti, *Phys. Chem. Chem. Phys.* 15, 9726 (2013).